Progress In Electromagnetics Research B, Vol. 74, 23–35, 2017

Parabolic Trail OBF in Magnetic Anomaly Detection

Yao Fan[2, *], Xiaojun Liu[2], and Guangyou Fang[1]

Abstract—Magnetic anomaly detection (MAD) is to find hidden ferromagnetic objects, and a hidden object is often described as a magnetostatic dipole. Many detection methods are based on the orthonormal basis functions when the target moves along a straight line relatively to the magnetometer. A new kind of parabolic trail orthonormal basis functions (PTOBF) method is proposed to detect the magnetic target when the trajectory of the target is parabola. The simulation experiment confirms that the proposed method can detect the magnetic anomaly signals in white Gaussian noise when SNR is −15.56 dB. The proposed method is sensitive to the characteristic time and curvature. High detection probability and simple implementation of proposed method make it attractive for the real-time applications.

1. INTRODUCTION

Magnetic anomaly detection (MAD) methods have been used for decades to detect ferromagnetic targets. Though before the technology is widely used in many cases, the range of detection is limited because of magnetic noise. In the past few years, there have been some noise reduction methods such as entropy filter [1], referenced magnetometer [2], high-order crossing method [3], orthonormal basis functions (OBF) matched filtering method [4, 5], and wavelet transform method [6–8]. In most research environments, it is assumed that the target moves along a straight line relatively to the magnetometer. Curve trajectory detection has essential value in these applications, just as pipeline flaw detection [9], intrusion detection [10], earthquake prediction [11]. The motion trail between the target and magnetometer is arbitrary, and the parabolic trail is the one of the simplest trails of the arbitrary trail, so it is important to discover the detection method when the motion trail between the target and magnetometer is parabola.

In this paper, a parabolic trail orthonormal basis functions (PTOBF) method is proposed to detect the magnetic target effectively when the trajectory of the magnetic target is a parabola, even the magnetic anomaly signal of the magnetic target is weak. Based on a parabolic target track dealt with in [2], here, we propose an analytic approach which enables to further investigate the influence of the curvature on the basis functions and on the detection performance. Anomalies will be revealed by a wave form or threshold. The proposed PTOBF method is tested to detect the weak signal in white Gaussian noise for −15.56 dB.

The remainder of this paper is organized as follows. In Section 2, we review the magnetic anomaly detection fundamental principle. The basic theoretical derivation of the PTOBF algorithm is described in Section 3. Section 4 presents the performance of the PTOBF by a series of simulation experiments and real-world experiments. Further work is considered in Section 5 followed by conclusions in Section 6.

Received 13 September 2016, Accepted 27 March 2017, Scheduled 5 April 2017

* Corresponding author: Yao Fan (fanyao14@mails.ucas.ac.cn).

[1] Key Laboratory of Electromagnetic Radiation and Sensing Technology, Chinese Academy of Sciences, Beijing 100190, People's Republic of China. [2] University of Chinese Academy of Sciences, Beijing 100039, People's Republic of China.

2. MAGNETIC ANOMALY DETECTION

In many cases, the magnetic target can be treated as a dipole, and the magnetic field produced by target may be considered as dipole field [12, 15].

$$\vec{B} = \frac{\mu_0}{4\pi} \frac{3\left(\vec{M}\cdot\vec{R}\right)\cdot\vec{R} - \vec{M}R^2}{R^5} \tag{1}$$

where μ_0 is the permeability of free space and $\vec{B}$ the magnetic induction field produced by a target with the moment of $\vec{M}$ at distance $\vec{R}$.

A magnetic sensor [13, 14] measures a net field composed of target magnetic induction field, earth field, and magnetic noise

$$\vec{B}_m = \vec{B} + \vec{B}_E + \vec{B}_n \tag{2}$$

The earth field $\vec{B}_E$ ranges between approximately 500 and 600 milligauss, and the variation is small. It can be regarded as the DC field and can be removed by the matlab's function detrend. $\vec{B}_n$ mainly comes from the shaking of the magnetometer, geomagnetic noises and sensor's intrinsic noise. When the magnetometer is stationary, the noise of magnetometer shaking is negligible. The geomagnetic noise is larger than sensor's intrinsic noise.

In this work, a three-axis fluxgate magnetometer is used to detect a moving small magnet.

3. THE PROPOSED PTOBF METHOD

The moving trail of the magnetic target relatively to magnetometer is demonstrated in Fig. 1.

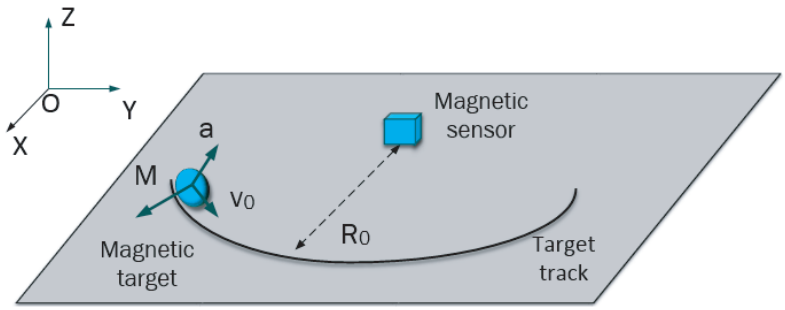

Figure 1. A vector magnetometer place to detect a magnetic dipole moving along a parabolic trail.

In our PTOBF method, we assume that the target will move along a parabolic trail. The magnetic sensor axes lie in the same plane with the target. In the Cartesian coordinate system, we assume that the magnetometer is displayed in the focus of the parabolic trail $(0, \frac{v_0^2}{2a})$, where v_0 is the horizontal speed and a the vertical acceleration of the target.

The target trail equation is presented by

$$\vec{r}(t) = v_0 t * \vec{x} + \frac{1}{2}at^2 * \vec{y} \tag{3}$$

The distance between the magnetometer and the target is given by

$$\vec{R}(t) = v_0 t * \vec{x} + \left(\frac{1}{2}at^2 - \frac{v_0^2}{2a}\right) * \vec{y} \tag{4}$$

We define $p = \frac{1}{2}at^2 - \frac{1}{2}\frac{v_0^2}{a}$, $q = \frac{1}{2}at^2 + \frac{1}{2}\frac{v_0^2}{a}$. Then we get the presentation

$$\vec{B}(t) = \frac{u_0}{4\pi}\left[\frac{3 * (m_x v_0 t + m_y p)\cdot(v_0 t, p, 0)}{q^5} - \frac{(m_x q, m_y q, m_z q)}{q^5}\right] \tag{5}$$

u and w are the dimensionless coordinate along the track of the target. It can be expressed by $u = \frac{at}{v_0}$, $w = \frac{v_0^2}{2a}$ and then

$$\vec{B}(u) = \frac{u_0}{4\pi}\frac{1}{w^5(1+u^2)^5}\left\{\begin{array}{c} 3m_y w^2u^3 + 12m_x w^2u^2 - m_x wu^2 - 3m_y w^2u - m_x w \\ \frac{3}{2}m_y wu^4 + 6m_x w^2u^3 - wu^2 - 6m_x w^2u + \frac{1}{2}m_y w - m_z(u^2+1)w \end{array}\right\} \quad (6)$$

If the sensor axes are not aligned with X and Y directions, there will be another equation of the magnetic anomaly signal. The rotation of the magnetometer is demonstrated by Fig. 2.

$$\left[\begin{array}{c} B_{xNew} \\ B_{yNew} \\ B_{zNew} \end{array}\right] = \frac{u_0}{4\pi}\frac{1}{w^5(1+u^2)^5}\left\{\begin{array}{c} (3m_y w^2u^3 + 12m_x w^2u^2 - m_x wu^2 - 3m_y w^2u - m_x w)\sin D\cos I \\ \left(\frac{3}{2}m_y wu^4 + 6m_x w^2u^3 - wu^2 - 6m_x w^2u + \frac{1}{2}m_y w\right)\cos D\cos I \\ (-m_z(u^2+1)w)\sin I \end{array}\right\} \quad (7)$$

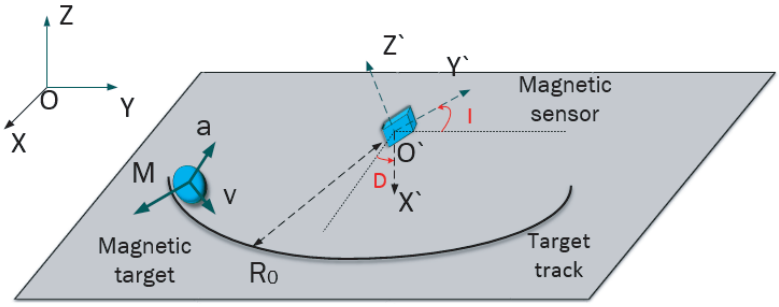

Figure 2. A vector magnetometer rotates in a certain angle of D and I.

Obviously, the magnetic target signal along the y axis of the sensors will be presented by five linearly independent basis functions $\Phi_i(u)$ for $i = 1, 2, 3, 4, 5$:

$$\Phi_1(u) = \frac{1}{(u^2+1)^5} \quad (8)$$

$$\Phi_2(u) = \frac{u}{(u^2+1)^5} \quad (9)$$

$$\Phi_3(u) = \frac{u^2}{(u^2+1)^5} \quad (10)$$

$$\Phi_4(u) = \frac{u^3}{(u^2+1)^5} \quad (11)$$

$$\Phi_5(u) = \frac{u^4}{(u^2+1)^5} \quad (12)$$

The functions are linearly independent as proved by a Wronskian matrix with a nonzero determinant

$$\left|\begin{array}{ccccc} \Phi_1 & \Phi_2 & \Phi_3 & \Phi_4 & \Phi_5 \\ \frac{d\Phi_1}{du} & \frac{d\Phi_1}{du} & \frac{d\Phi_1}{du} & \frac{d\Phi_1}{du} & \frac{d\Phi_1}{du} \\ \frac{d^2\Phi_1}{du^2} & \frac{d^2\Phi_2}{du^2} & \frac{d^2\Phi_3}{du^2} & \frac{d^2\Phi_4}{du^2} & \frac{d^2\Phi_5}{du^2} \\ \frac{d^3\Phi_1}{du^3} & \frac{d^3\Phi_2}{du^3} & \frac{d^3\Phi_3}{du^3} & \frac{d^3\Phi_4}{du^3} & \frac{d^3\Phi_5}{du^3} \\ \frac{d^4\Phi_1}{du^4} & \frac{d^4\Phi_2}{du^4} & \frac{d^4\Phi_3}{du^4} & \frac{d^4\Phi_4}{du^4} & \frac{d^4\Phi_5}{du^4} \end{array}\right| = \frac{288}{(u^2+1)^{25}} \neq 0 \quad (13)$$

We strive to build a set of bases functions $\Psi_i(u)$ and fulfill the orthogonalization.

$$\Psi_1(u) = \frac{1}{(u^2+1)^5} \tag{14}$$

$$\Psi_2(u) = \frac{u}{(u^2+1)^5} \tag{15}$$

$$\Psi_3(u) = \frac{u^2}{(u^2+1)^5} - \frac{1}{17}\frac{1}{(u^2+1)^5} \tag{16}$$

$$\Psi_4(u) = \frac{u^3}{(u^2+1)^5} - \frac{1}{5}\frac{u}{(u^2+1)^5} \tag{17}$$

$$\Psi_5(u) = \frac{u^4}{(u^2+1)^5} - \frac{6}{13}\frac{u^2}{(u^2+1)^5} + \frac{1}{65}\frac{1}{(u^2+1)^5} \tag{18}$$

The energy of the functions is shown in Table 1. It is clear that $\|\Psi_1(u)\|$ and $\|\Psi_2(u)\|$ have larger value than two times of $\|\Psi_3(u)\|$, $\|\Psi_4(u)\|$, $\|\Psi_5(u)\|$, $\Psi_1(u)$ and $\Psi_2(u)$ which are the principle components of all five basis functions, but for the entire detection, we use all of them to construct the detector.

Table 1. The energy of the five basis functions.

$\|\Psi_1(u)\|$	$\|\Psi_2(u)\|$	$\|\Psi_3(u)\|$	$\|\Psi_4(u)\|$	$\|\Psi_5(u)\|$
$\sqrt{12155pi/65536}$	$\sqrt{715pi/65536}$	$\sqrt{429pi/278528}$	$\sqrt{33pi/81920}$	$\sqrt{3pi/16640}$
0.7633	0.1851	0.0696	0.0356	0.0238

And then normalize

$$g_1(u) = \sqrt{\frac{65536}{12155\pi}}\frac{1}{(u^2+1)^5} \tag{19}$$

$$g_2(u) = \sqrt{\frac{65536}{715\pi}}\frac{u}{(u^2+1)^5} \tag{20}$$

$$g_3(u) = \sqrt{\frac{278528}{429\pi}}\left(\frac{u^2}{(u^2+1)^5} - \frac{1}{17}\frac{1}{(u^2+1)^5}\right) \tag{21}$$

$$g_4(u) = \sqrt{\frac{81920}{33\pi}}\left(\frac{u^3}{(u^2+1)^5} - \frac{1}{5}\frac{u}{(u^2+1)^5}\right) \tag{22}$$

$$g_5(u) = \sqrt{\frac{16640}{3\pi}}\left(\frac{u^4}{(u^2+1)^5} - \frac{6}{13}\frac{u^2}{(u^2+1)^5} + \frac{1}{65}\frac{1}{(u^2+1)^5}\right) \tag{23}$$

The orthonormal bases $g_1(u), g_2(u), g_3(u), g_4(u), g_5(u)$ are depicted by Fig. 3.

Optimal filter theory states that for the detection of a finite duration function $g_j(n), j = 1, 2, 3, 4, 5$ contaminated by white Gaussian noise, match filters with impulse response of $g_j(-n)$ are necessary. Then detection can be performed by using five matched filters by $g_j(-n), j = 1, 2, 3, 4, 5$, and the output will be $h_j(n), j = 1, 2, 3, 4, 5$. The decision index is formed:

$$E(n) = \sum_{i=1}^{5} h_i^2(n) \tag{24}$$

Detection occurs when the decision index value exceeds a predetermined threshold, as depicted in Fig. 4.

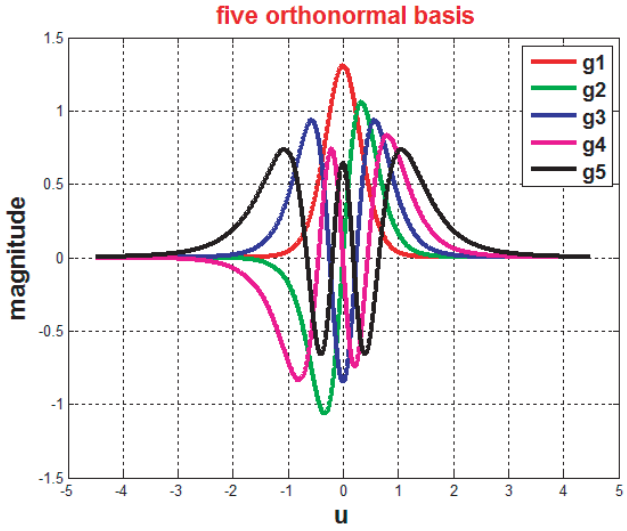

Figure 3. Normalized orthogonal basis $g_1(u), g_2(u), g_3(u), g_4(u), g_5(u)$.

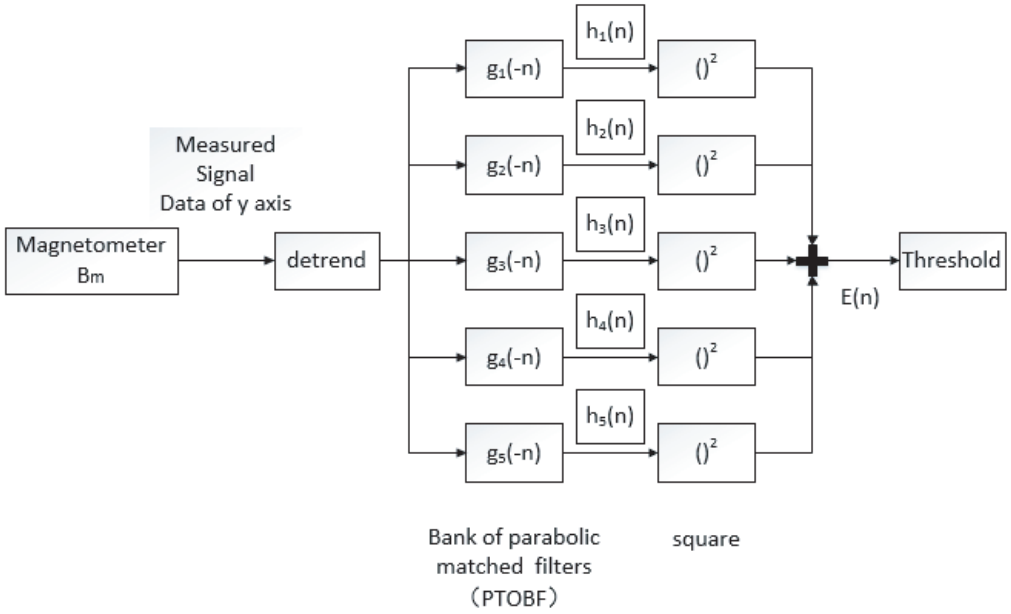

Figure 4. Magnetic target detection scheme using PTOBFs.

4. SIMULATION AND REAL-WORLD EXPERIMENT OF THE PTOBF METHOD

4.1. Simulation of the PTOBF Method

This section presents the performance evaluation of the proposed method. The parameters of the simulation experiment are shown in Table 2. At time $t = 0$, the closest proximity approach (CPA) is 0.9 m between the magnetometer and the target. We assume that the speed of the target is 3 m/s and that the acceleration of the target is 5 m/s^2. The magnetic moment of the target is $(1, 0, 0)$. The sampling frequency is 100 Hz.

The three components of the magnetic anomaly signal are depicted in Fig. 5. We assume that the moment is existent towards the x-axis. And in the simulation, SIN $I = 0$. So according to formula (7) the scalar of the z-axis is always zero. Signal in x-axis is even symmetry, and the maximum magnitude

Table 2. Parameters of the simulation experiment.

Symbol	Quantity	Value	Units
m	target magnetic moment	$(1, 0, 0)$	$\mathrm{A \cdot m^2}$
V	target velocity	3	m/s
a	target acceleration	5	$\mathrm{m/s^2}$
CPA	closest proximity approach	0.9	m
τ	characteristic time	0.3	s
Cu	curvature	1.333	$\mathrm{s^{-1}}$
Ts	Sampling period	0.1	s

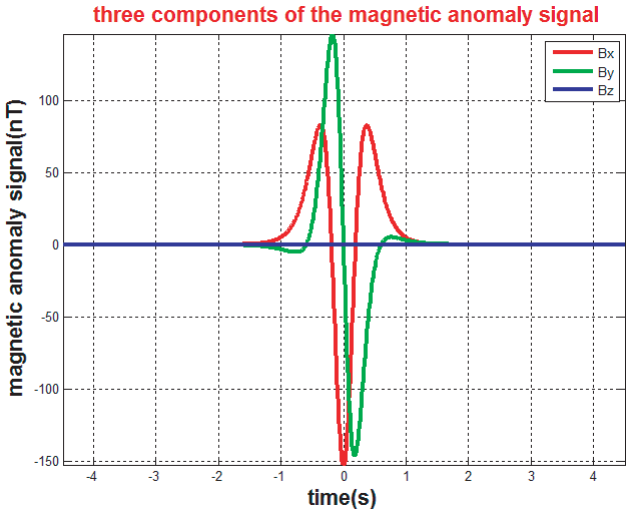

Figure 5. Three components of the magnetic anomaly signal.

of the anomaly signal is 150 nT. Signal in y-axis is odd symmetry, and the maximum magnitude of the anomaly signal is 148 nT. The sum of magnetic field value is even symmetry, and the maximum magnitude of the anomaly signal is 150 nT.

Then x-axis scalar of the signal is buried into the white Gaussian noise. For each value of the variance of noise σ^2, a simulated noise is generated. The noise and signal are depicted in Fig. 6. The signal-noise ratio (SNR) of each figure is -15.5612 dB, -10.044 dB, -4.5267 dB, -0.3888 dB, respectively.

The proposed PTOBF method is used to detect the signal, and the result is shown in Fig. 7.

When the SNR is -15.5612 dB, there are interferences beside the center position of signal. The output of the detector shows that the SNR is increased to -0.91 dB. When the SNR is -10.044 dB, interferences beside the center position of signal decreases obviously, and the SNR is increased to 2.95 dB. When the SNR is -4.5267 dB, interferences beside the center position of signal further decreases, and the SNR is increased to 12.95 dB. When the SNR is -0.3888 dB, interferences nearly disappears, and the SNR is increased to 24.57 dB.

In the simulation, we use a prior knowledge of the characteristic time and curvature, which in practice can rarely be predicted. Hence, a guess of characteristic time and curvature is required, or else a multichannel approach should be adopted. Fig. 8 shows the response of the detector as a function of various characteristic time values. Fig. 9 shows the response of the detector as a function of various curvature values. Fig. 10 shows the response of the detector as a function of both various curvature values and various characteristic time values.

The Monte Carlo method is also used to find the relationship between the detection probability,

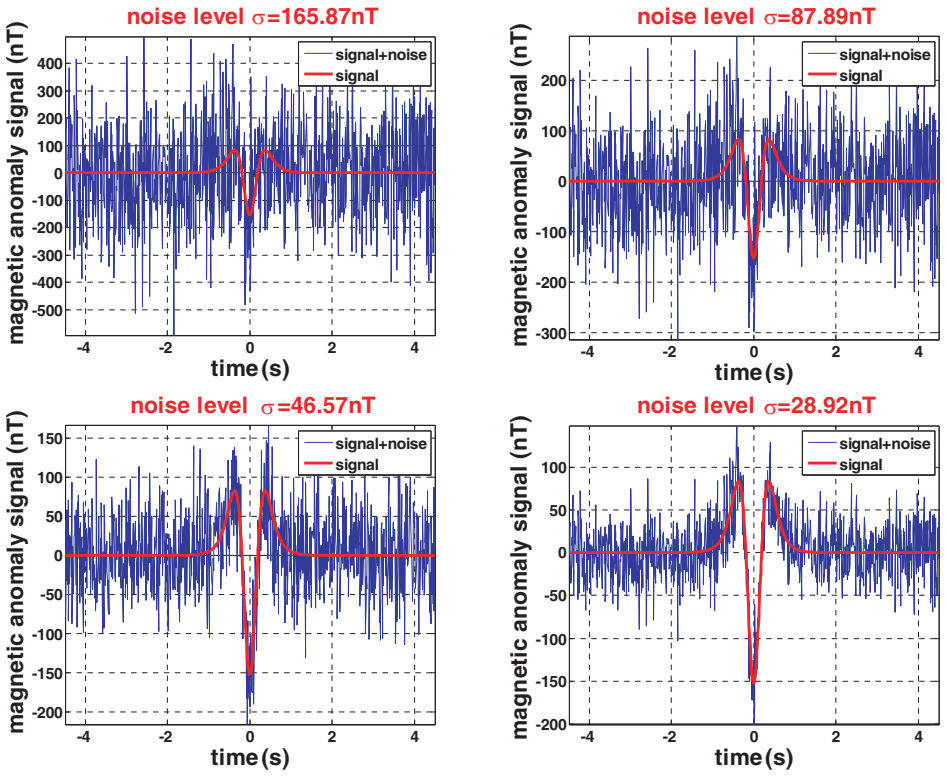

Figure 6. Magnetic anomaly signal is buried in white Gaussian noise.

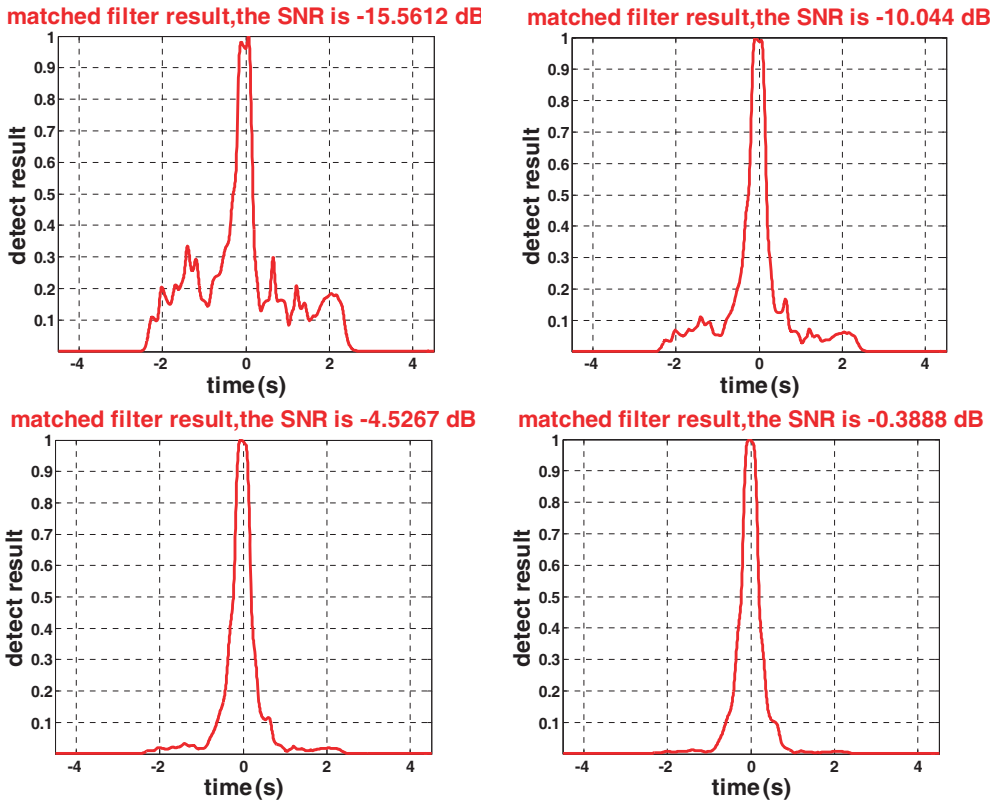

Figure 7. The detect result by PTOBF method.

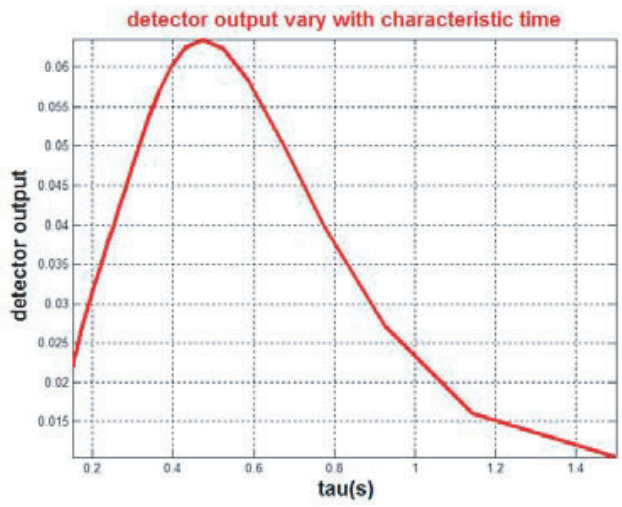

Figure 8. Typical response of detector for various characteristic time values. The peak coincides with the actual target characteristic time of 0.5 s.

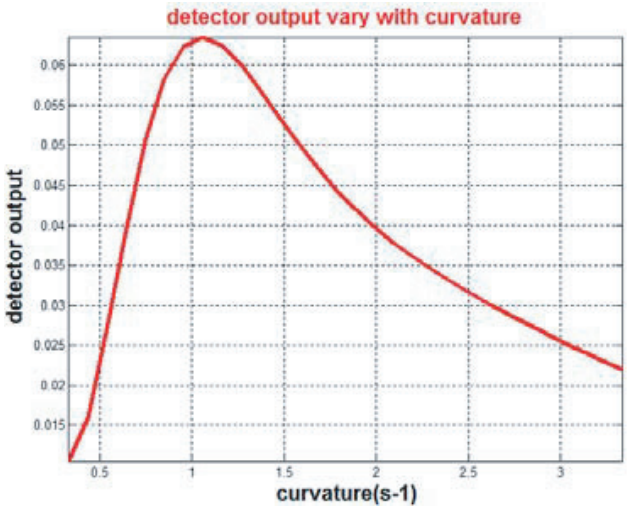

Figure 9. Typical response of detector for various curvature values. The peak coincides with the actual target curvature of about 1.1 s^{-1}.

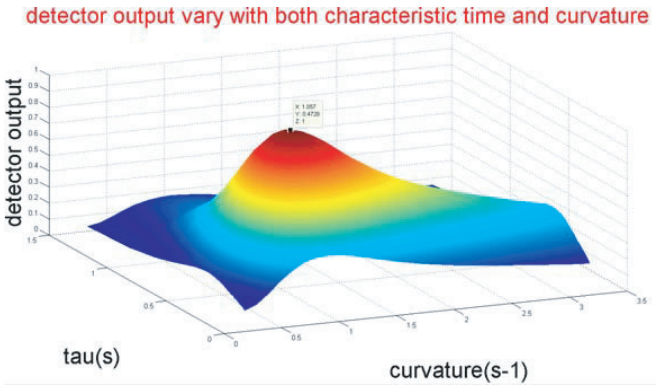

Figure 10. Typical response of detector for both various curvature values and various characteristic time values The peak coincides with the actual target curvature of about 1.1 s^{-1} and the characteristic time of 0.5 s.

false probability and signal-noise ratio (SNR). The process is repeated for 10000 times, each time with a renewed noise realization. The statistics of the detection and false times is calculated over the repetitions. The statistical result is depicted in Fig. 11 and Fig. 12.

It is likely to see that when the SNR is more than 0 dB, the proposed method can detect the target magnetic anomaly signal accurately. When the SNR is −5 dB, the detection probability is about 90%, and the false probability is about 10%. Even when the SNR is −15 dB, there are more than 50% probability to detect the target. The detection effect rapidly deteriorates when the SNR is lower than −15 dB.

4.2. Real-World Experiment

Experiments have been carried out in Beijing, and the apparatus and layouts of the experiment are illustrated in Fig. 13. The small magnet serves as a magnetic anomaly target. The magnetic sensor is Bartington's three-axis fluxgate sensor Mag-03MSL100 whose noise level is 6 $pT/\sqrt{Hz}$@1 Hz, frequency range 0 Hz–3 kHz, and its conversion factor 0.1 mV/nT. All the experiments are collected by the acquisition system NI with the sampling frequency of 100 Hz. The actual sampling rate should be

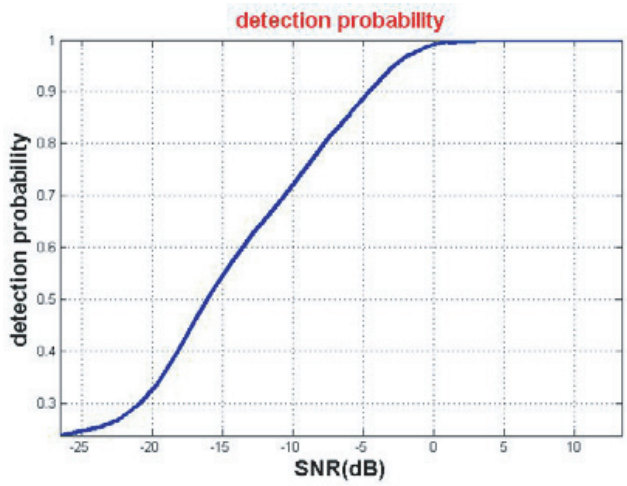

Figure 11. Detection probability.

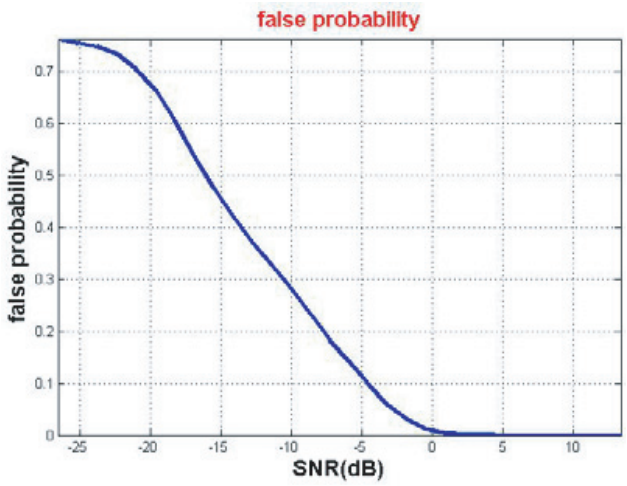

Figure 12. False probability.

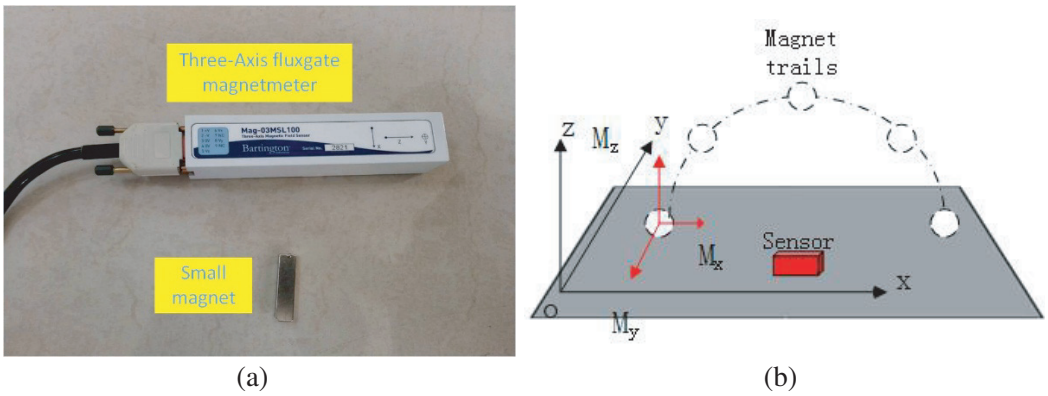

(a) (b)

Figure 13. The apparatus and layouts of the experiment.

higher than Nyquist sampling rate at a suitable value. The magnetic noise is from the geomagnetic background. Magnetic noise is stochastic, and its frequency bandwidth covers the signal's bandwidth. So the signal contains a certain amount of in-band noise. The received signals are intensely interfered by the magnetic noise in time and frequency domain.

In Section 3, the signal model is theoretical. The procedure of the target detection is shown in Fig. 14, mainly including the preprocessing, matched filtering, and threshold detection. In preprocessing, whether the entire data are effective should be confirmed first. After that, singular points should be removed, then the function detrend is used to handle the data. Secondly, a low-pass filter is used to cancel the noise in the high frequency. Thirdly, the data are input in the bank of parabolic matched filters. Fourthly, the corresponding signal energy is obtained by component matching. Finally, after calculating the sum of squares and normalized, a certain threshold is used to detect the existence of the target. The threshold value is determined using the Neyman-Pearson criterion [16]. This criterion can achieve maximal detection probability under a constraint on the false alarm rate. In order to get a false alarm once for 10^5 samples, the Neyman-Pearson criterion is used to determine a threshold about 0.07 when the added zero mean Gaussian white noise with $\sigma^2 = 0.002\,\mathrm{nT}^2$.

The required magnetic anomaly data are shown by Fig. 15. According to the electromagnetic theory, the low frequency magnetic field value decreases inversely proportional to the distance when the target can be deemed as one point source. The target appears at about 3 s but under the influence of geomagnetic background noise.

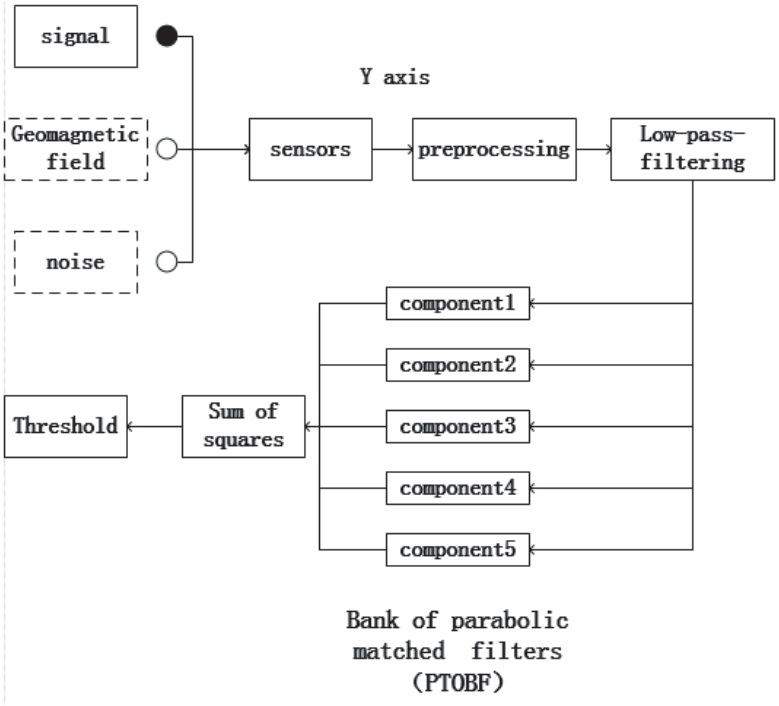

Figure 14. The procedure of signal processing.

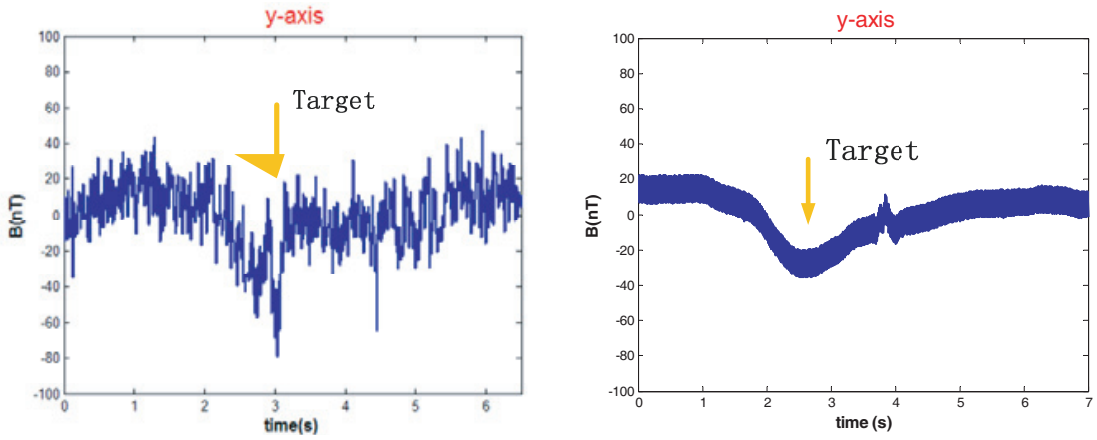

Figure 15. Record of experiment target signal (in the middle of the window).

Then the result of PTOBF method is shown in Fig. 16. It is turned out that the present approach based on the decomposition of the MAD in the space of orthonormal basis functions allows substantial advance in solving the parabolic trail detection problem. It is seen that even for unconspicuous target signal, the output energy of the detector is great at the time of magnetic anomaly target's appearance.

Traditional OBF method is also used to detect the target, and the detector output of traditional OBF method is shown in Fig. 16. In the application, the parameter of target is unknown. If the guessed velocity and closest proximity approach cannot match the real target, the traditional OBF method cannot work well in parabolic trail. Compared to traditional OBF method, the PTOBF perform well in parabolic trail target detection. For example, the target appears at 3.1 s and 2.7 s. The output of the PTOBF detector locates the target accurately. Simultaneously, the PTOBF method is used for strict parabolic trail according to formula (6). If the target moves in other trails, the PTOBF method becomes invalid.

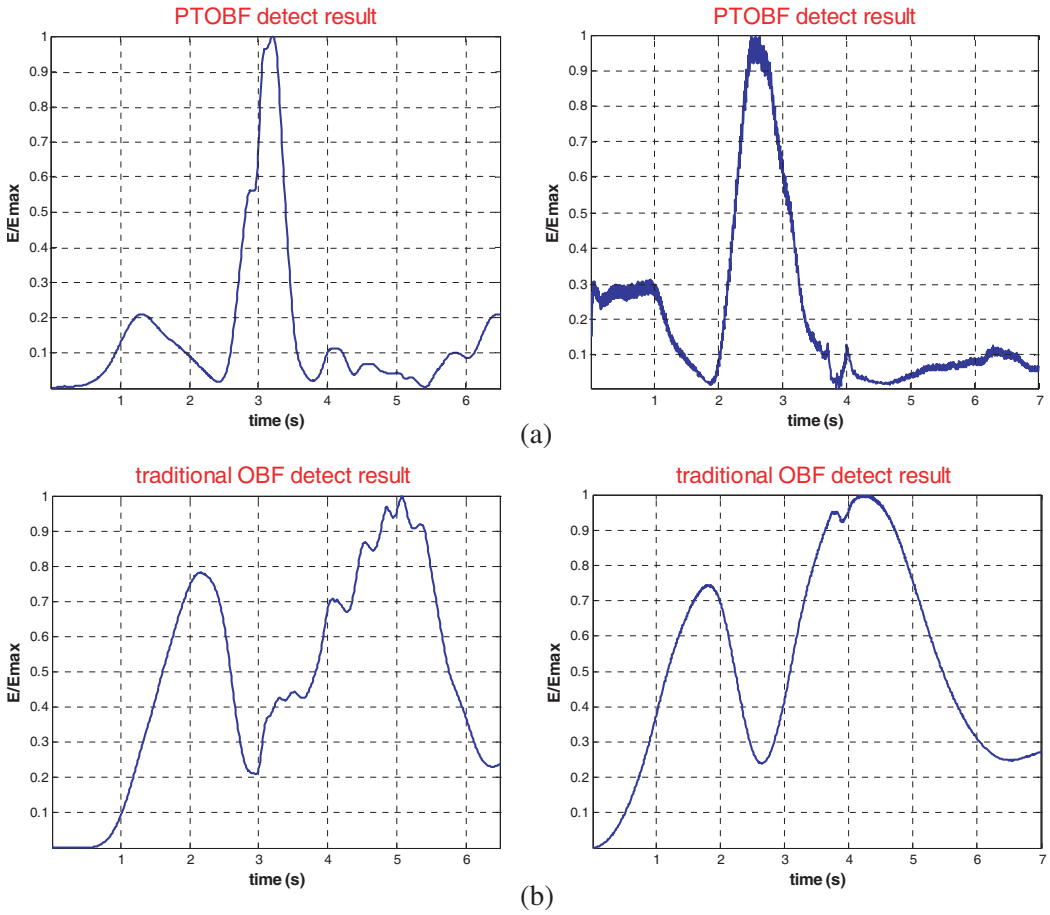

Figure 16. (a) The corresponding detector output. The PTOBF detect output. (b) The traditional OBF detect output.

5. FURTHER WORK

The parabolic trail is just a special example of the arbitrary trail. Next, we will research the circle trail or hyperbolic trail OBF method or combine such several kinds of methods to detect arbitrary trail.

6. CONCLUSIONS

In this work, parabolic trail orthonormal basis function (PTOBF) method is proposed to detect the target when the trajectory of the target is a parabola. The results show high detection probability even for low SNR values. Compared to traditional OBF method, the PTOBF method performs well in parabolic trail. The detector is sensitive to the characteristic time and curvature. The real-world experiment result confirms that it is effective to detect the target. The positive result indicates that PTOBF method is a potential candidate for MAD.

ACKNOWLEDGMENT

This research is sponsored by the National High Technology Research and Development Program of China (Grant No. 2014AA093407) and the National Natural Science Foundation of China (Grant No. 41374186).

APPENDIX A.

Parabolic trail orthonormal basis functions algorithm parameters acronyms list.

$\vec{B}$: magnetic induction field.
$\vec{B}_E$: earth geomagnetic field.
$\vec{B}_n$: magnetic noise.
μ_0: the permeability of free space.
$\vec{M}$: the target magnetic moment.
R: the distance between target and magnetometer sensor.
R_0: the closest proximity approach between target and magnetometer sensor.
v_0: the target initial velocity.
a: the target acceleration.
u: characteristic time.
w: the trail curvature.
$\Phi_i(u)$: linearly independent basis functions.
$\Psi_i(u)$: orthogonalized basis functions.
$g_i(u)$: orthonormal basis functions.
$h_i(n)$: the output of each matched filter.
$E(n)$: the decision index.

REFERENCES

1. Sheinker, A., N. Salomonski, B. Ginzburg, et al., "Magnetic anomaly detection using entropy filter," *Measurement Science & Technology*, 19, 2008.
2. Sheinker, A., L. Frumkis, B. Ginzburg, et al., "Magnetic anomaly detection using a three-axis magnetometer," *IEEE Transactions on Magnetics*, Vol. 45, 160–167, 2009.
3. Sheinker, A., B. Ginzburg, N. Salomonski, et al., "Magnetic anomaly detection using high-order crossing method," *IEEE Transactions on Geoscience and Remote Sensing*, Vol. 50, 1095–1103, 2012.
4. Sheinker, A., B. Lerner, N. Salomonski, et al., "Localization and magnetic moment estimation of a ferromagnetic target by simulated annealing," *Measurement Science & Technology*, Vol. 18 3451–3457, 2007.
5. Yu, H., S. Feng, and L.-H. Wu, "Synchronous correction of two three-axis magnetometers using FLANN," *Sensors and Actuators A — Physical*, Vol. 179, 312–318, 2012.
6. Nie, X., Z. Pan, D. Zhang, et al., "Energy detection based on undecimated discrete wavelet transform and its application in magnetic anomaly detection," *Plos One*, Vol. 9, e110829–e110829, 2014.
7. Nie, X. H., Z. M. Pan, and W. N. Zhang, "Wavelet based noise reduction for magnetic anomaly signal contaminated by $1/f$ noise," *Advanced Materials Research*, Vol. 889–890, 776–779, 2014.
8. Zhou, J. J., C. S. Lin, and Y. C. Huan, "Decreasing noise in magnetic anomaly detection basing on wavelet denoising," *Applied Mechanics & Materials*, Vol. 368–370, 1860–1863, 2013.
9. Ke, M., P. Liao, and X. Song, "Real-time data mining in magnetic flux leakage detecting in boiler pipeline," *International Conference on Digital Manufacturing & Automation*, Vol. 2, 130–133, 2010.
10. Wang, Y., Weihuang F, and D. P. Agrawal, "Intrusion detection in Gaussian distributed wireless sensor networks," *IEEE International Conference on Mobile Adhoc & Sensor Systems*, 313–321, 2009.
11. Zubaidah, T., B. Kanata, C. Ramadhani, et al., "Comprehensive geomagnetic signal processing for successful earthquake prediction," 212–219, 2013.
12. Sheinker, A., A. Shkalim, N. Salomonski, et al., "Processing of a scalar magnetometer signal contaminated by $1/f^{\alpha}$ noise," *Sensors & Actuators A Physical*, Vol. 138, 105–111, 2007.

13. Ma, J. S., J. Jiao, C. Fang, et al., "High sensitive nonlinear modulation magnetoelectric magnetic sensors with a magnetostrictive metglas structure based on bell-shaped geometry," *Journal of Magnetism and Magnetic Materials*, Vol. 405, 225–230, 2016.
14. Morag, Y., N. Tal, M. Nazarathy, et al., "Thermodynamic signal-to-noise and channel capacity limits of magnetic induction sensors and communication systems," *IEEE Sensors Journal*, Vol. 16, 1575–1585, 2016.
15. Zhang, H. and M.-Y. Xia, "Magnetic anomaly detection for simultaneous moving target and magnetometer," *Proceedings of 2014 3rd Asia-Pacific Conference on Antennas and Propagation (APCAP 2014)*, 884–888, IEEE, 2014.
16. Kay, S. M., *Fundamentals of Statistical Signal Processing: Detection Theory*, Printice Hall PTR, 1998.